Lab on a Chip

PAPER

View Article Online
View Journal

Cite this: DOI: 10.1039/d5lc01050k

High-recovery AAV clarification using a multiplexed spiral inertial microfluidic platform

Alexander Bevacqua, [abc] Do Hyun Park,[b] Sheryar Khan,[d] Qingxuan Li,[d] Mahsa Hadidi,[d] Jianzhu Chen[ce] and Jongyoon Han *[abf]

The clinical adoption of emerging cell and gene therapies relies on the efficient upstream bioprocessing and high-recovery harvesting of viral vectors. AAV purification from cell culture begins with the removal of cells, through a process called cell clarification, which is typically performed with a membrane filter. Cells and debris accumulate on the filter matrix during clarification, resulting in filter clogging and significant product loss. Here, we implement spiral inertial microfluidic technology as an alternative, membraneless clarification strategy to separate AAVs from the host cells. We assemble a parallelized plastic spiral microfluidic system that divides an input flow rate of cell culture across 100 spirals to harvest clarified material at 20 mL min^{-1}. The microfluidic clarification platform achieves a viral vector recovery of 85%, with the additional 15% of recoverable AAVs remaining in the system. However, up to 20% of cells were also found in the harvest, signifying that cell removal by inertial clarification is incomplete. We incorporate spiral microfluidics with the 3M Harvest RC filter (0.2 μm) (3M, USA) into a two-step harvest process, where spiral microfluidic clarification is used first to remove most of the cells from the culture. Performing spiral microfluidic clarification before depth filtration improves the filter throughput by 56.25%, from 44.8 L m^{-2} to 70 L m^{-2} and leads to a two-step AAV recovery of ~74%, exceeding the 40 to 70% clarification recoveries generally reported. Our results support that further optimization and scale-out of the spiral inertial microfluidic system could increase the overall clarification recovery of AAV production processes.

Received 14th November 2025,
Accepted 7th May 2026

DOI: 10.1039/d5lc01050k

rsc.li/loc

1. Introduction

Viral vector manufacturing serves a pivotal role in cell and gene therapy formulation and production, and it is one of the most critical bottlenecks due to the explosive growth in clinical trials.[1–4] The efficient production and harvesting of viral vectors, such as adeno-associated virus (AAV) vectors, is essential to advance novel gene therapy products into clinical usage. The upstream manufacturing process often involves host cell cultures (such as HEK293), followed by transfection, to produce AAVs. Vandenberghe *et al.* report that the distribution of intracellular and extracellular AAVs 72 hours post-transfection depends on serotype and other process parameters such as the presence or absence of serum in culture media.[5] To maximize product yields, at the start of downstream processing, intracellular AAVs are released from producer cells either by cell lysis[6] or in a lysis-free manner by shifting cell culture conditions (such as pH and temperature) to facilitate the release of AAVs into the supernatant.[7] For example, sub-lethal cellular stresses such as raising the pH from 7.2 to 8.0 increases the overall release of AAVs from the cells to the supernatant (from 0% presence in the supernatant at pH 7.2 to 92% presence in the supernatant at pH 8.0).[7] Downstream processing steps such as depth filtration, tangential flow filtration, affinity chromatography, anion-exchange chromatography, ultrafiltration, and diafiltration into an appropriate storage buffer are performed to isolate the AAV product from cells, proteins, nucleic acids, and other debris and impurities.[6] Many of these unit operations used in viral vector bioprocessing were adapted from those used in monoclonal antibody downstream processing.[6] Filtration is considered the most costly of these unit operations, and it is the primary contributor to losses in functional viral titers.[8]

The cells that are used to produce viral vectors are commonly removed from solution using a depth filter through a process called cell clarification, where cells and

[a] *Department of Biological Engineering, Massachusetts Institute of Technology, Cambridge, Massachusetts, USA. E-mail: jyhan@mit.edu*
[b] *Research Laboratory of Electronics, Massachusetts Institute of Technology, Cambridge, Massachusetts, USA*
[c] *Koch Institute for Integrative Cancer Research, Massachusetts Institute of Technology, Cambridge, Massachusetts, USA*
[d] *Genomic Medicine Unit, Purification Process Development, Sanofi R&D, Waltham, Massachusetts, USA*
[e] *Department of Biology, Massachusetts Institute of Technology, Cambridge, Massachusetts, USA*
[f] *Department of Electrical Engineering and Computer Science, Massachusetts Institute of Technology, Cambridge, Massachusetts, USA*

other larger debris are entrapped on a filter matrix with sub-micron-sized pores. These matrices are designed to allow viral vectors to pass through the pores. During filtration, the accumulation of cells leads to filter clogging, which poses a persistent problem that substantially reduces product recovery.[9] In a viral vector manufacturing workflow with cell lysis and nuclease treatment, it has been previously reported that overall AAV recovery lowers from 85% to 38% during the initial clarification step with a 1.2 μm filter, and overall recovery lowers further from 38% to 28% with the second clarification step involving a two-stage 0.8 μm/0.2 μm filter.[10] The AAV recoveries of each of these unit operations are 44.7% and 73.7%, respectively. Another team reports a 72% two-step recovery of AAV8 from the clarification of batch cultures after lysis and nuclease treatment using a 5.0 μm filter, followed by a two-stage 0.8 μm/0.2 μm filter.[11] In their perfusion culture runs, they report clarification recoveries between 15% and 97%, with an average of 50% recovery across their runs.[11] The two studies referenced here employ several filtration steps in series with progressively lower pore sizes, aiming to minimize excessive cell build-up on any one filter, which can reduce undesired product retention and allow the burden of clarification to be shared across multiple filtration units.[10,11]

Cell clarification devices that can support industry-scale processes with high vector recoveries are crucial to making AAV-based gene and cell therapies accessible to patients. Spiral inertial microfluidic technology is an emerging alternative to membrane-based filtration, offering a label-free, size-based, membraneless, and continuous clarification strategy.[12–14] Previous studies have highlighted the effectiveness of using spiral inertial microfluidic technology to hydrodynamically control various entities, including immune cells, tumor cells, antibody-producing Chinese hamster ovary (CHO) cells, and bacteria.[12–14] The technology has potential applicability in the biomanufacturing space due to its ability to hydrodynamically focus cells towards one outlet, while allowing biological products to passively exit through the other outlet, effectively separating them.[12–14] Size-dependent inertial focusing of micron-sized cells is possible with spiral microfluidic technology due to a combination of Dean and lift forces perpendicular to the direction of flow, which equilibrate cells to a position near the inner wall of the spiral.[12–14] Antibody harvesting from CHO cell culture has previously been demonstrated with this technology due to the size differences between CHO cells and antibodies.[12–14] We previously utilized spiral microfluidic technology as a cell retention device for lentiviral vector perfusion bioprocessing;[15] however, its application to AAV downstream processing and purification has not been reported. At the start of downstream processing, if cells are lysed to release their intracellular AAVs, introducing the cells' subcellular components in the mixture can complicate the AAV purification process. Instead, after performing a cell culture shift to non-lethally release intracellular AAVs into the supernatant,[7] subsequent downstream processing steps such as microfluidic clarification can be performed on whole cells. Therefore, total vector yields from clarification with the spiral microfluidic device would depend in part on the extent in which the producer cells release vectors to the supernatant. For example, AAV9 and lentiviral vectors are predominantly released out of the cell,[16] removing the need for lysis, while AAV2 is primarily kept intracellularly.[5]

A single spiral channel made from polydimethylsiloxane (PDMS) is only capable of accepting 5 to 10 mL min^{-1} of cell culture fluid with a harvest stream outputting 0.5 mL min^{-1} (or 720 mL per day) of material.[14] To ensure that spiral inertial microfluidic technology is scalable for larger industry-scale batch processes or perfusion bioreactors of several liters or even hundreds of liters, parallelization of spiral channels is necessary. Dividing a 1 L min^{-1} input flow rate across 100 spiral channels in parallel, for example, would equal a 10 mL min^{-1} per spiral input flow rate. Parallelizing the field of inertial microfluidics was first achieved with a multiplexed PDMS device, where layers of PDMS devices, each with 4 spirals, were stacked on top of one another.[13] This device operated at a 240 mL min^{-1} total input flow rate.[13] PDMS multiplexed spiral inertial microfluidic technology has several drawbacks, including a labor-intensive fabrication process and susceptibility to channel deformations caused by higher pressures and flow rates, which can negatively impact separation performance. To overcome these challenges, we have previously designed a mass-producible, injection-molded, plastic spiral microfluidic device comprising four spiral channels that operate in parallel.[12] The individual injection-molded devices can be stacked on top of one another to form a multiplexed unit with the number of spirals equal to four times the number of layers in the stack.[12]

In this study, we investigate the utilization of spiral inertial microfluidic technology, an alternative to conventional harvesting strategies such as centrifugation or membrane filters, as a new unit operation for the downstream processing and recovery of AAVs from non-lysed, human producer cell culture. Using a spiral device comprising 100 spirals operating in parallel, we recover AAVs at a rate of 20 mL min^{-1} with a mean vector recovery of 85.1%, accompanied by minimal cell breakthrough (3 to 7%) during the first 80% of the run. When spiral microfluidic clarification is used before depth filtration, it improves the throughput of the filter by 56.25% and leads to a second-stage AAV recovery of 84.9%.

2. Experimental methods

2.1. Cell clarification platform – microfluidic device fabrication

Polycarbonate spiral devices were injection molded using master molds that were previously fabricated at RnD Factory, South Korea, so that they are mass-producible and inexpensive (<$1 per device).[12] A single device (1 layer with 4 spirals) is shown in Fig. 1(a). Each spiral has 4 loops, and its

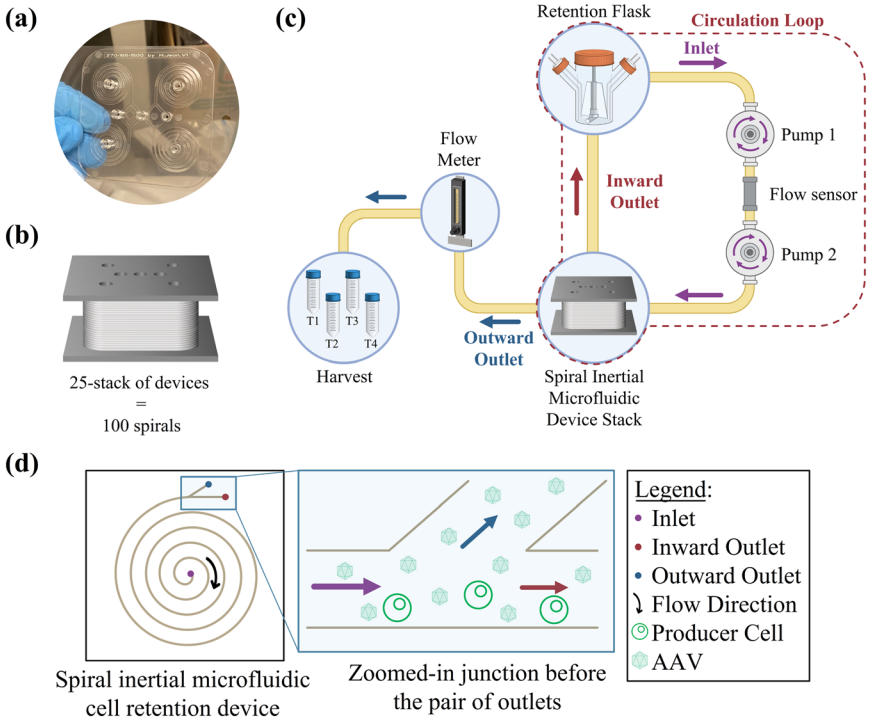

Fig. 1 (a) A photograph of a single polycarbonate spiral inertial microfluidic device. (b) An illustration of a 25-layer device compressed between two metal plates. (c) The flow path of the cell clarification circulation platform. Material from the cell retention flask is pumped into the spiral inertial microfluidic device stack at a rate of 1000 mL min^{-1}, which is continuously monitored by a flow sensor. A flow meter maintains the flow rate of the harvest stream at 20 mL min^{-1}. A clarified solution is collected into different conical tubes throughout the run, allowing measured cell densities and AAV titers to be associated with a specific point in time. (d) An illustration of the separation junction dividing an inlet flow (purple arrow) into the inward outlet (red arrow) and outward outlet (blue arrow). Cells are inertially focused towards the inward outlet, while viral vectors are continuously harvested through the outward outlet, as their motion is not influenced by inertial focusing.

trapezoidal cross-section has a base of 1500 μm, an inner wall height of 270 μm, and an outer wall height of 165 μm.[12] A high-throughput cell clarification platform, similar to the one described in Jeon *et al.*,[12] was assembled by stacking 25 polycarbonate devices (for a total of 100 spirals). To ensure that the device layers are precisely aligned with one another, they were stacked using an aluminum pin holder, whose rods align with the entry holes of each device.[12] During the stacking process, the layers are bonded to one another by double-sided adhesive films. The assembled stack of devices is illustrated in Fig. 1(b) and then secured between a pair of stainless steel plates using bolted joints, to ensure that no leaks occur between the layers of the platform.[12]

2.2. Cell clarification platform – circulation system setup

The circulation system illustrated in Fig. 1(c) is assembled and pictured in Fig. 2. A spinner flask (Corning, USA), where the unprocessed, pre-clarification material is located initially, is placed on a stirrer plate (SS2I, Corning, USA). During the experiments, the stirring rate was set to 60 rotations per minute (rpm) to maintain continuous mixing of the cell retention flask contents. Two pumps (PuraLev® i100MU, Levitronix, USA) were positioned in series downstream from the spinner flask and operated together to achieve a 1 L min^{-1} inlet flow rate into the microfluidic device. The input flow rate is measured continuously using an external, clamp-on flow sensor (LFSC-i16X-001, Levitronix, USA) located between the two pumps. Using Levitronix – Service Software V2.0.7.0 to control the pumps, the rpm setpoints were determined using Process Mode. Process Mode was set to 5%, which autonomously adjusts the input flow rate to 1 L min^{-1} (5% of the pumps' maximum) and adjusts the rpm as needed to maintain the proper flow rate. The inlet of the spiral microfluidic device was outfitted with a pressure sensor to monitor the inlet pressure. The input flow rate is divided into four streams, corresponding to the four inlet holes at the top of the 25-layer stack of microfluidic devices. These are illustrated as the four purple arrows entering the device stack in Fig. 2. The outward outlet is connected to a flow meter (6A0109BV-WA, Dakota Instruments, Inc., USA) to control the volumetric flow rate of the harvest stream.

2.3. Cell clarification platform – cleaning

Before each experiment, the flow path was cleaned, as many of the parts could not be sterilized individually by autoclaving. 500 mL of 10% bleach in sterilized water was flowed through the system at a rate of 1000 mL min^{-1}. The contents of the retention flask are removed using an

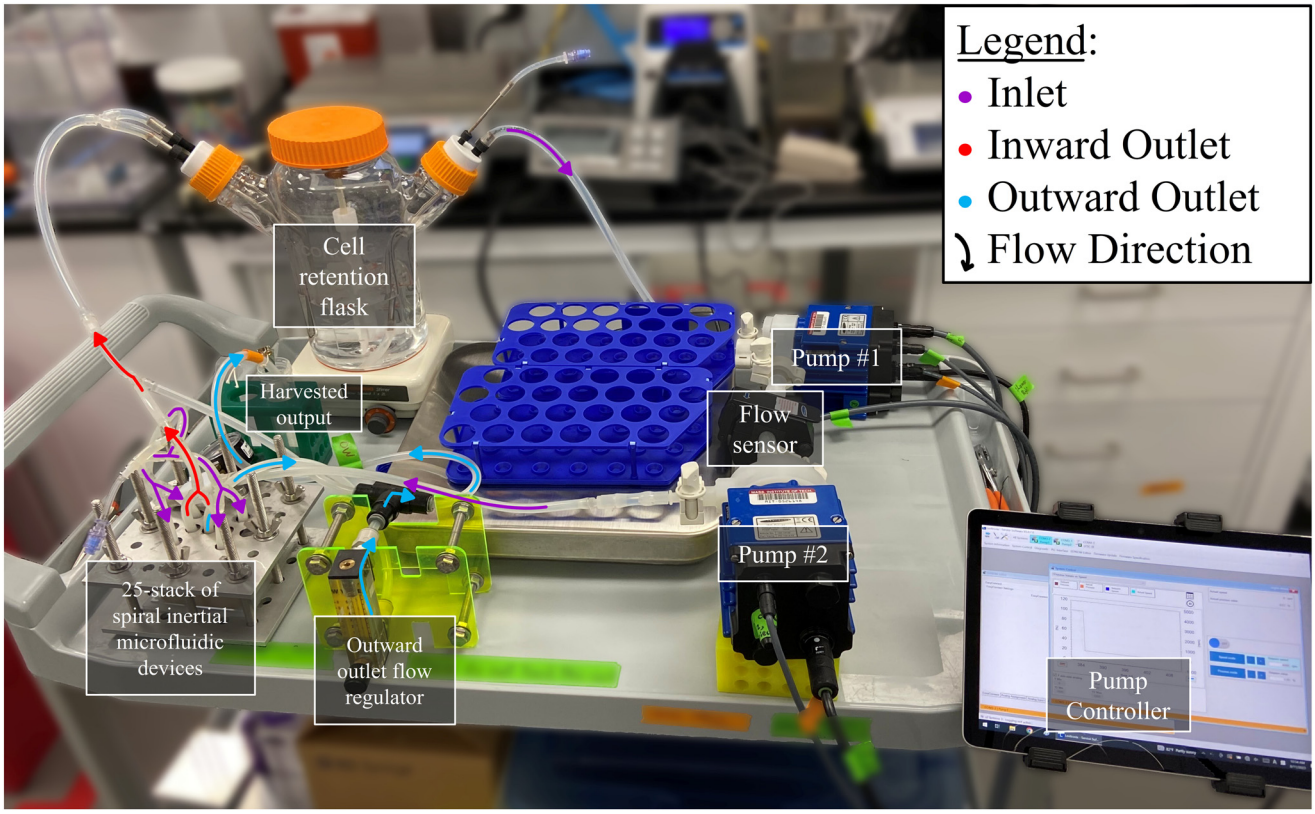

Fig. 2 The circulation system with the flow path illustrated. The two pumps transfer cell culture material from the cell retention flask to the inlet of the spiral microfluidic device stack (indicated by purple arrows). The device (25-layer, 100 spirals in parallel) accepts an input flow rate of 1000 mL min^{-1} and harvests 20 mL min^{-1} of material through the flow meter (blue arrows). It returns the remaining cell culture fluid, along with the inertially focused cells, through the inward outlet (red arrows) back to the cell retention flask, allowing it to be mixed and pumped back to the inlet once more.

aspiration pipette, ensuring that no bubbles are introduced into the circulation loop. Then, the flow path was flushed with 500 mL of sterile water three times and then 500 mL of phosphate-buffered saline (PBS) five times. This protocol was developed to ensure the complete removal of cells, cell debris, and bleach from the flow path before a run. To maintain cell integrity and appropriate tonicity conditions during each experiment, the cell clarification platform's flow path was filled with PBS before each run. A new spiral device stack was assembled before each run.

2.4. AAV harvesting runs – experimental design for microfluidic clarification

Human producer cell culture material (500 mL for Experiment 1, 800 mL for Experiment 2, and 480 mL for Experiment 3, respectively) was deposited into the cell retention flask. The material was first pumped at 1000 mL min^{-1} through the circulation loop for 1 minute without harvesting to create an inertial focusing equilibrium within the stack of 25 spiral microfluidic devices.

Once harvesting began, each experiment had a unique sampling plan. The feedstock was circulated at a rate of 1000 mL min^{-1} to maintain an optimal flow rate of 10 mL min^{-1} per spiral.[12] A harvest flow rate of 20 mL min^{-1} was maintained through the outward outlet of the device stack using a flow meter. Samples collected at different points in time throughout the harvesting routine were referred to as time fractions. This was done to better understand the distribution of cells and AAVs throughout the clarification run. These samples would be used to measure the cell density, viral titer, and turbidity at a precise point in time within the harvesting routine at one of several locations of interest, which include the outward outlet (the harvest stream), the inward outlet (the retentate stream in the circulation loop), and the cell retention flask. Viral titer measurements were done by quantitative PCR (qPCR), cell density and viability measurements were done using the Vi-Cell XR (Beckman Coulter, USA), and turbidity measurements were taken using the 2100Q Portable Turbidimeter (Hach, USA).

Experiment 1 consisted of 25 evenly spaced time fractions, each comprising 20 mL of samples. Of the 20 mL taken, 15 mL was collected through the outward outlet of the spiral device, 2.5 mL was withdrawn from the inward outlet using a syringe, and 2.5 mL was withdrawn from the cell retention flask using a syringe. Experiment 2 consisted of 40 evenly spaced time fractions, each comprising 20 mL of samples,

which offered more temporal resolution on the harvesting process than the first experiment. Of the 20 mL taken, 18 mL was collected through the outward outlet of the spiral device, and 2 mL was withdrawn from the cell retention flask by syringe. Experiment 3 consisted of one time fraction where 250 mL of harvest material was collected from the outward outlet, and 23 time fractions of 10 mL were collected from the outward outlet thereafter. Each sample was tested for its cell density, viral titer, and turbidity according to the assay plans in Tables S1–S3 for Experiments 1 through 3, respectively.

2.5. Depth filter throughput study

A depth filter throughput study was conducted to determine the throughput (in L m^{-2}) of the Harvest RC (HRC) BC25, a commercially available, single-stage purification unit (3M, USA). The BC25 Sanitary unit from the HRC series has a 25 cm^2 filter surface area with a 0.2 μm membrane.[17] A representative sample of microfluidic-clarified material from Experiment 3 with a turbidity of less than 300 Nephelometric Turbidity Units (NTUs) (the first 320 mL of harvest) was compared with an unprocessed cell culture (sourced from the same batch) that had not undergone microfluidic clarification. In both conditions, material was delivered through the BC25 at a flux of 100 L m^{-2} per hour[18] (100 LMH, which corresponds to a volumetric flow rate of 4.17 mL min^{-1}). Throughput is defined as $\frac{V}{25\ cm^2}$, commonly converted to L m^{-2}, where V is the volume of material that was processed with the HRC before the inlet pressure reaches the safety ceiling of 5 psi.

2.6. Computational fluid dynamics simulations

COMSOL Multiphysics Version 6.3 was used to perform simulations of inertial focusing with a 25-layer spiral microfluidic device. This was done to characterize the velocity and pressure profiles and acquire particle tracing visualizations to support the experimental results. Since the assembled device is symmetrical along two perpendicular axes, two symmetry nodes were added to the model builder to simplify the workflow. The complete profile was then regenerated by symmetry. In all simulations, the volumetric flow rate of the inlet was 10 mL min^{-1} per spiral and the harvest flow rate through the outward outlet was 0.2 mL min^{-1} per spiral. For particle tracing results, the particles were assigned a uniform size of 20 μm. More details on the calculations are in the SI.

3. Results and discussion

3.1. Low cell breakthrough to the harvest stream

The goal of microfluidic cell clarification as a unit operation in a downstream processing harvest train is to harvest AAVs while simultaneously retaining cells in the circulation loop, as illustrated in Fig. 1(c). Inertial focusing is a size-dependent phenomenon in spiral microfluidics, and its effect on micron-scale cells and nanometer-scale AAVs is summarized and illustrated in Fig. 1(d). Further details on single spiral channel inertial focusing of suspension cells can be found in earlier works.[12–15] The spiral geometry and separation mechanism in this work closely follow the work by Jeon *et al.* on the clarification of CHO cells to harvest antibodies using a multilayered geometry.[12] When cell culture feedstock is introduced into the multilayered spiral microfluidic device stack, the spiral geometry within each layer enables Dean flow vortices to form, and the cells equilibrate to a position near the inner wall, predominantly exiting the spiral device through the inward outlet.[12–15] The hydrodynamic regime is laminar, and it is characterized using calculations of the Reynolds number and the Dean number, which are reported in the SI. Since the multilayered spiral microfluidic clarification device must be compressed between two metal plates to withstand the inlet pressure without leakage, real-time microscopy of the focusing bands within each device layer is not possible. A computational fluid dynamics particle tracing simulation of the 25-layer device sorting 20 μm diameter spheres, which are intended to represent producer cells, is viewable in Video S1. The residence time of cells in the device is less than 0.4 seconds. AAVs are dispersed throughout the channel and are too small to undergo inertial focusing, which allows them to be harvested through the outward outlet. This is congruent with other studies that demonstrate that particles with sizes under 1 μm such as lentiviral vectors,[15] viruses,[19] and nanoparticles[20] are not inertially focused, and can therefore be passively harvested through the outward outlet. The outward outlet of the spiral device is 1500 μm wide, which, when contrasted with the sub-micron-sized pores of membrane-based filters, eliminates the possibility of device clogging.

To achieve high clarification efficiency, the outward outlet of the microfluidic device stack, which leads to the harvest stream and collection tube, should have as small a cell breakthrough as possible. In Fig. 3(a), the cell density in the outward outlet (harvest stream) at 25 distinct, equally spaced points in time (named time fractions) is shown. The cell clarification efficiency is a measure of how proficiently the spiral microfluidic device sorts cells into the inward outlet.

Cell clarification efficiency is defined as

$$\text{Cell Clarification Efficiency} = 100\% - \frac{\text{Outward Outlet Total Cell Density}}{\text{Retention Flask Total Cell Density}}$$

The lower the cell breakthrough into the outward outlet, the higher the cell clarification efficiency.[12–14] Cell clarification efficiency depends on the flow rates into and through the device, the device's dimensions, and the cell density in the circulation loop.

A representative result is shown in Fig. 3(a), which corresponds with the assay plan shown in Table S1

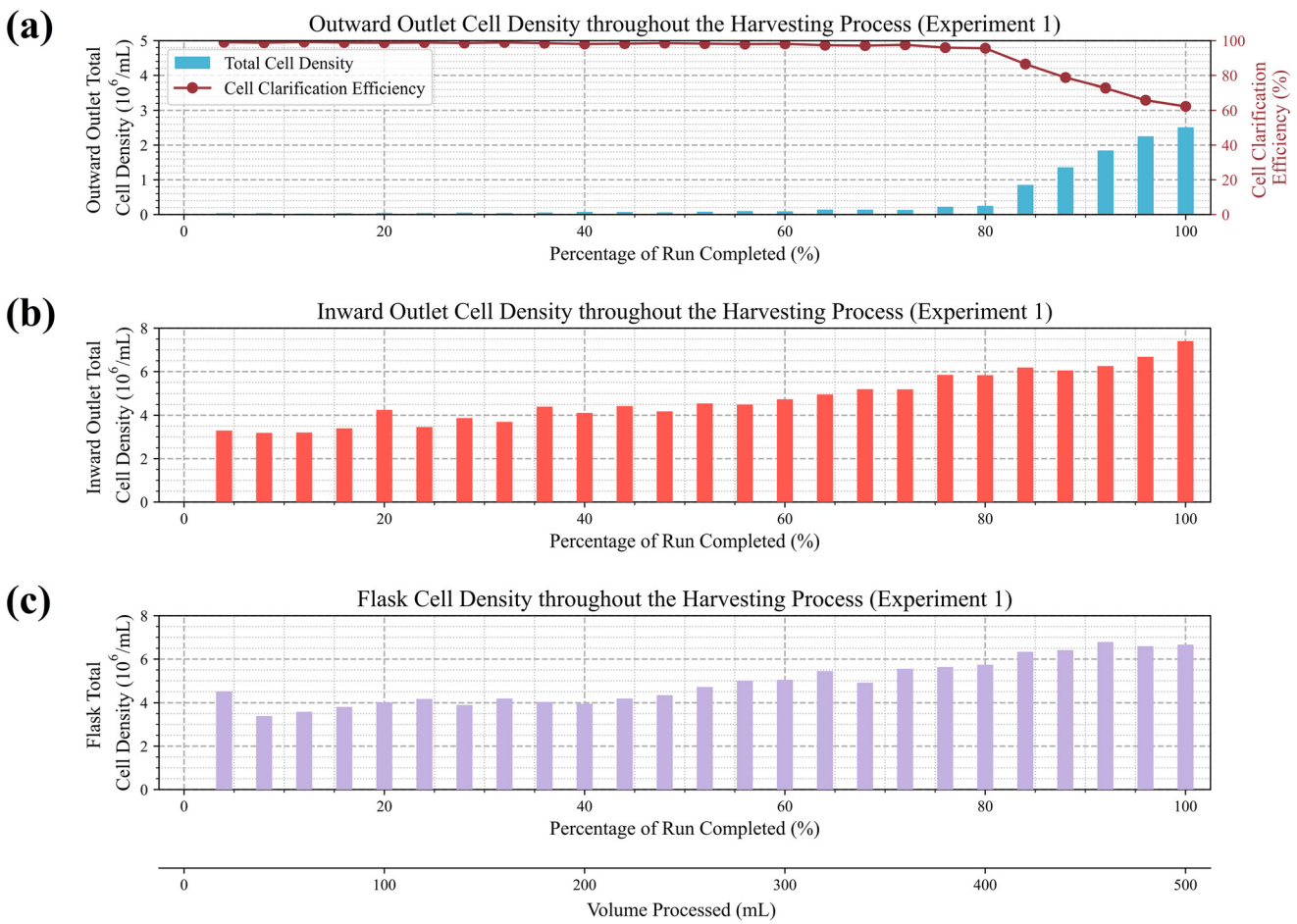

Fig. 3 (a) The total cell density of the samples collected from the outward outlet measured at 25 points during the harvest of 500 mL of cell culture, as well as the spiral device's clarification efficiency during this process. (b) and (c) The total cell density of the samples in (b) the inward outlet of the spiral device and (c) the cell retention flask.

(Experiment 1, 500 mL of unprocessed material, 25 time fractions). The initial total cell density in the flask was 4.51×10^6 cells per mL, with a 3.2% viability. The results show that the vast majority of AAVs were found in the supernatant.

The runs yielded reproducible results, with cell densities as low as 4×10^4 cells per mL as a harvest breakthrough at the start of the runs, corresponding to a 99.1% cell clarification efficiency. The device retained cells in the circulation loop as AAVs were harvested through the outward outlet, and as the volume in the cell retention flask decreased, the cell densities recorded in the cell retention flask and the inward outlet of the spiral device rose.

In Fig. 3(a), the total cell density of the outward outlet samples was less than 5×10^5 cells per mL up until time fraction 20 of 25, or 80% of the run, and the cell clarification efficiency was 95.6% or higher up to that point. The cell densities of the samples taken at the inward outlet and the retention flask are reported in Fig. 3(b) and (c), respectively. The spiral device begins to perform less efficiently at the point when around 80% of the run is complete (or in other words, when 400 mL of the 500 mL has been processed in Fig. 3(a)), and the cell clarification efficiency begins to decrease due to the rising cell density in the circulation loop. Two additional runs (Experiments 2 and 3, see Fig. S1 and S2, Tables S2 and S3) show a largely similar trend.

The results reveal that cell clarification efficiency depends on the cell density in the circulation loop (*i.e.*, retention flask). This would loosely correlate cell clarification efficiency to the percentage of total cell culture volume processed. As long as the cell density in the circulation loop (or retention flask) remains below a certain threshold ($\sim 6 \times 10^6$ cells per mL), we expect clarification efficiency to remain over 95% until approximately 80% of the run is complete, regardless of the initial starting volume.

Additionally, as another metric of device performance, turbidity measurements were taken during each of the microfluidic clarification experiments. The outward outlet samples were the only ones that produced a reading of less than 1000 Nephelometric Turbidity Units (NTUs) (Fig. S3). They follow the trend of the outward outlet cell density readings since the removal of cells contributes to a lowering of turbidity. In contrast, the inward outlet and retention flask readings exceeded the instrument's readable range. These initial feedstocks had a higher turbidity than crude pre-

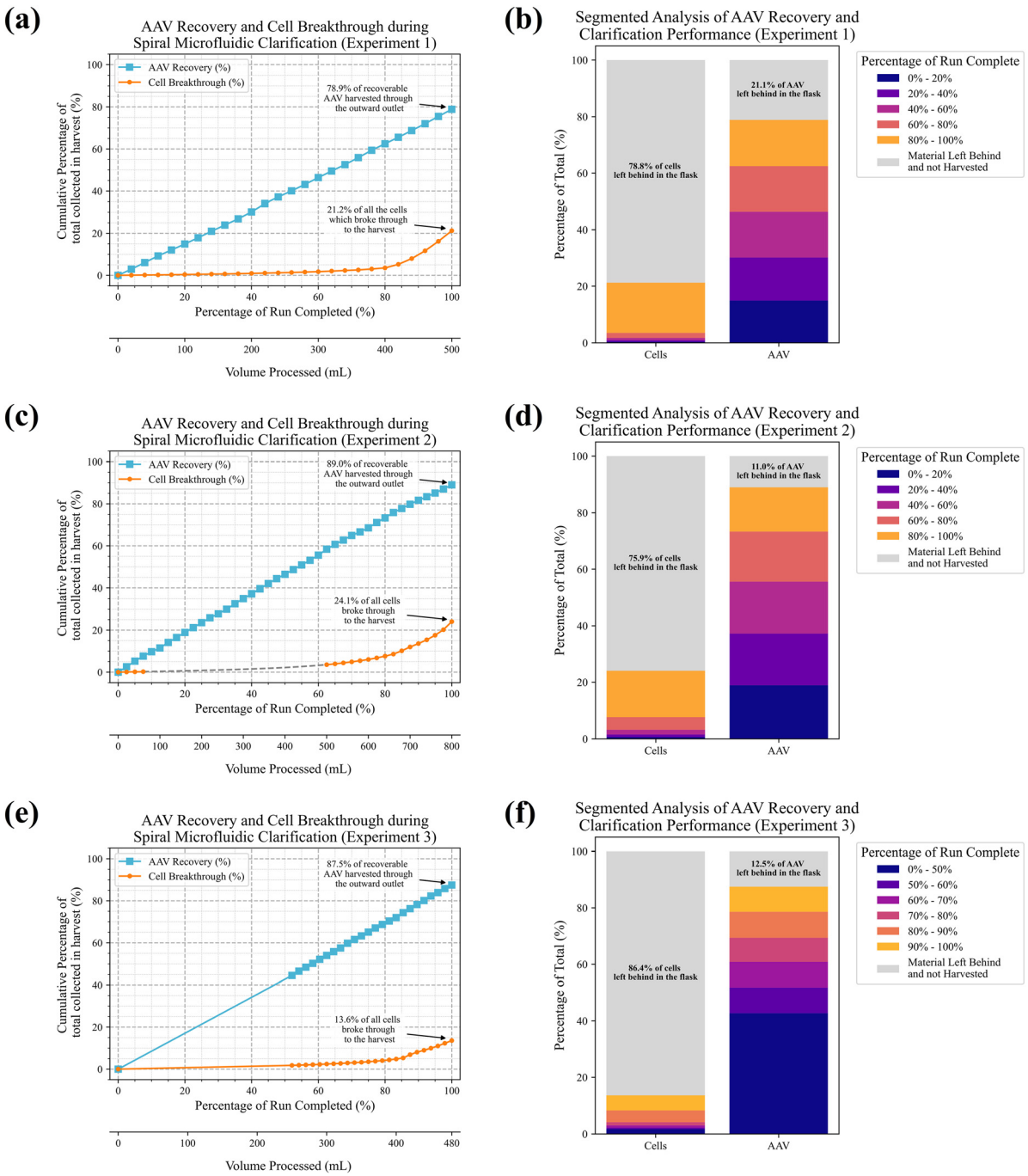

Fig. 4 (a) AAV recovery and cell breakthrough during spiral microfluidic clarification in Experiment 1, where 500 mL of cell culture was processed to obtain an AAV recovery of 78.9% and a total cell breakthrough of 21.2%. (b) The AAV recovery and cell breakthrough in Experiment 1 were temporally resolved to highlight the AAV collections and cell breakthrough at different points in the run. 21.1% of the AAVs and 78.8% of the cells were left behind once spiral microfluidic clarification was completed. (c) AAV recovery and cell breakthrough during spiral microfluidic clarification in Experiment 2, where 800 mL of cell culture was processed to obtain an AAV recovery of 89.0% and a total cell breakthrough of 24.1%. Cell density measurements were not taken from time fractions 4 to 24 (10% to 60% of the run completed), according to the sampling plan in Table S2. During this interval, the total cell density in the outward outlet samples increased from 3.5×10^4 cells per mL to 1.6×10^5 cells per mL. An exponential curve fit (grey dashed line) was used to infer the total cell densities (Fig. S5). (d) The AAV recovery and cell breakthrough in Experiment 2 were temporally resolved to highlight the AAV collections and cell breakthrough at different points in the run. 11.0% of the AAVs and 75.9% of the cells were left behind once spiral microfluidic clarification was completed. (e) AAV recovery and cell breakthrough during spiral microfluidic clarification in Experiment 3, where 480 mL of cell culture was processed to obtain an AAV recovery of 87.5% and a total cell breakthrough of 13.8%. Note that the first non-zero measurement is representative of the first 250 mL of harvest material through the outward outlet. (f) The AAV recovery and cell breakthrough in Experiment 3 were temporally resolved to highlight the AAV collections and cell breakthrough at different points in the run. 12.5% of the AAVs and 86.4% of the cells were left behind once spiral microfluidic clarification was completed. A detailed description of the methodology used to calculate the cumulative AAV recovery and the cumulative cell breakthrough as a function of the percentage of the run completed is in the SI.

clarification collections from lysed adherent culture of AAV5, 8, and 9 (~70 to 190 NTUs)[21] and AAV-producing lysed suspension cultures of AAV8 and 9 (~200 to 900 NTUs).[22]

3.2. High-throughput and high-recovery AAV harvesting

For each of the three harvesting runs, clarification was performed with a harvest flow rate of 20 mL min^{-1}, and in addition to measuring cell densities, viral titers were measured from samples sourced from the cell retention flask, inward outlet, and outward outlet as described in the assay plans shown in Tables S1–S3. Genomic titer measurements for each time fraction were performed using qPCR and are reported in Fig. S4. Within each experiment, the measured titers remained relatively stable over time and between sample sources (*i.e.*, the retention flask, the inward outlet, and the outward outlet), which was expected since AAVs are theoretically unaffected by inertial focusing.

Fig. 4 shows AAV recovery and cell breakthrough levels to the outward outlet throughout the harvesting process for the three experiments. Fig. 4(a), (c) and (e) show these results on a cumulative basis from the start of these runs until completion. The average AAV recovery is 85.1% and the average total cell breakthrough is 19.6%. Fig. 4(b), (d) and (f) divide all the recoverable AAVs and cells into distinct segments of the run. For example, the cell breakthrough in the final 20% of the run (between 80% and 100% of run completion) is far greater than the cell breakthrough at the earlier points of the run. In Experiment 3, where 13.6% of cells were in the harvest, 4.2% of cell breakthrough occurred between the 0% to 80% mark, and 9.4% of cell breakthrough occurred between the 80% to 100% mark. In Experiment 2, inertial cell focusing stability is inferred, rather than directly measured, during the central portion of the clarification run, specifically between time fractions 4 to 24 (10% to 60% of the run completed) as seen in Fig. 4(c). Cell clarification efficiency lowered from 98.8% to 96.4% during this interval.

There are slight variations in the genomic titers measured in each sample collected during microfluidic clarification, but the overall trend of cumulative vector genome recovery is linear with R^2 = 0.9997 in Experiment 1 (Fig. 4(a)), R^2 = 0.9993 in Experiment 2 (Fig. 4(c)), and R^2 = 0.9998 in Experiment 3 (Fig. 4(e)). This suggests, as hypothesized, that AAVs are not influenced by inertial focusing to travel down a specific outlet of the spiral device, and that the AAVs are passively collected at an approximately constant rate. This is consistent with other nanometer-scale biological products that do not inertially focus through the inward outlet, as seen in other works focusing on antibody production from CHO cells.[12–14] The linear relationship between cumulative AAV recovery and time also shows that there is minimal AAV loss to the plastic spiral microfluidic channels themselves.

Once the retention flask is sufficiently drained to the point where air could risk entering the tubing and disrupt the separation efficiency, the run is stopped. A fraction of the recoverable AAVs remains in the cell culture fluid occupying the tubing and the microfluidic device. These were considered unrecovered AAVs when reporting the overall recoveries in Fig. 4. On average, 14.9% of the AAVs and 80.4% of the cells were left behind in the circulation system. Those remaining AAVs are recoverable beyond the reported recoveries, and the simplest practical solution to continue a harvesting routine with the same microfluidic device stack is to add more unprocessed cell culture or fresh cell culture media to the cell retention flask. By adding more culture volume regularly during a harvesting run, the retention flask would not become empty, so harvesting can continue without introducing air bubbles into the circulation loop. The overall cell density in the loop would be lowered, which will lower cell breakthrough through the outward outlet and improve cell clarification efficiencies above the levels reported in this work. We expect that the AAVs remaining in suspension within the tubing of the circulation loop and channels of the device are recoverable since they are not entrapped in a filter matrix with our membraneless device. Realistically, by adding more cell culture media or culture volume to continue spiral microfluidic clarification, the overall recovery is expected to rise to between 90% and 95%. The one drawback of this strategy is that the AAVs would be diluted in a volume that is greater than the pre-clarification volume of cell culture.

3.3. Trade-off between cell clarification efficiency and AAV recovery

Conventional membrane-filtration-based cell clarification achieves near-complete cell removal from the harvest, but inevitably leads to cell clogging, membrane fouling, and related product loss that could amount to approximately 20 to 65%, depending on the conditions of the feed and membrane materials.[10,23] Inertial microfluidic cell clarification processes introduced in this work, in contrast, enjoy a high product recovery of at least 85% (with the possibility of achieving even higher by collecting the remaining recoverable AAVs from the fluid volume occupying the circulation loop's tubing), but at the expense of cell breakthrough into the harvest stream if the cell density is raised above a critical threshold. Fig. 5 illustrates the compromise between the high AAV recoveries that are achievable and the cell breakthrough that will accompany it.

The total number of AAV viral genomes (vg) that could be harvested by microfluidic clarification varied between the three experiments due to differences in the total volumes processed and cell-specific productivities. Non-ideal spiral device performance is observed near the end of a clarification run, where additional collection of AAVs is accompanied by an undesirable increase in cell breakthrough, as shown using the data of Experiment 1 in Fig. 5(a). The moment where the cumulative cell breakthrough exceeds 10^5 cells per mL approximately corresponds to the moment when cumulative cell breakthrough exceeds 5% (overall cell clarification falls below 95%) in all three experiments. Before this point, 4.68 × 10^{12} vg (Experiment 1), 8.11 × 10^{13} vg (Experiment 2), and

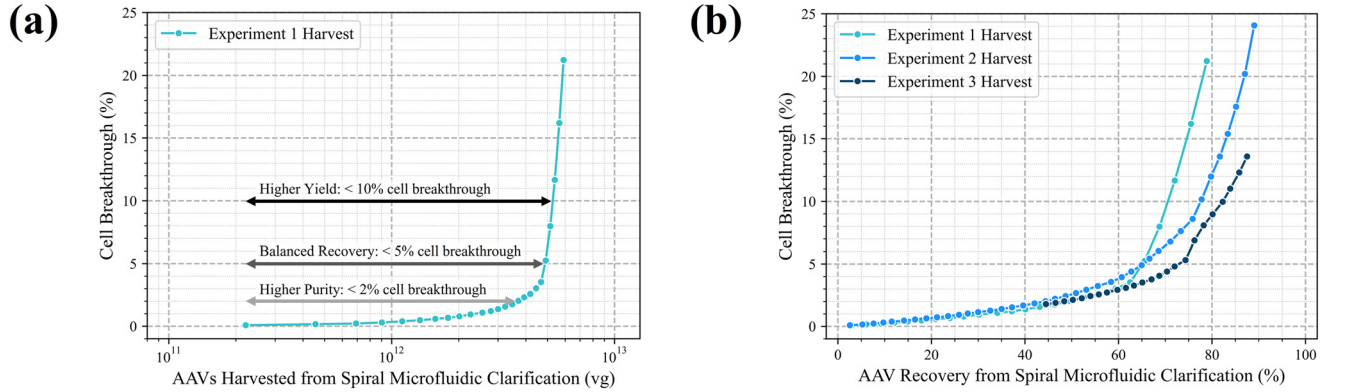

Fig. 5 (a) Cumulative cell breakthrough as a function of AAV viral genomes (vg) harvested during microfluidic clarification, using Experiment 1 as a representative dataset. Since spiral microfluidics is used for primary clarification, operating regions with under 2%, under 5%, and under 10% cell breakthrough are illustrated, showing the relationship between purity, yield, and anticipated biomass loading for secondary clarification. (b) Cumulative cell breakthrough as a function of AAV recovery. Since Experiments 1 and 2 demonstrated that the beginning of the experiment has the highest device performance, in Experiment 3, the first sample measured represents the first 250 mL of harvest material, containing 44.5% of the AAVs and 1.8% of the cells.

2.56×10^{13} vg (Experiment 3) were collected in the harvest stream. The specific operating window, which defines an acceptable degree of cell breakthrough from primary clarification given AAV recovery, depends on the capacity of subsequent clarification stages (such as secondary filtration) to fully remove the remaining cell biomass. The cutoff to this operating window may be set at 2%, 5%, 10%, or 15% cell breakthrough or defined based on measured cell densities in the harvest stream. These thresholds are simply illustrative, rather than generally validated operating criteria.

The relationship between AAV recovery and cell breakthrough is shown in Fig. 5(b). Since cell breakthrough is primarily caused by the rising cell density in the circulation loop, one way to continue AAV harvesting with minimal cell breakthrough is by maintaining the cell density in the circulation loop constant. Using Experiment 1 as an example, by adding cell culture material continuously to maintain the flask cell density at 4×10^6 cells per mL, a harvest cell breakthrough under 4×10^4 cells per mL, and a cell clarification efficiency of 99%, AAV harvesting can continue with minimal cell breakthrough to achieve higher recoveries and higher total viral genomes. There is no limit on the volume of material that can be processed with the spiral device, so this could theoretically continue in perpetuity.

To describe the performance illustrated in Fig. 5(b) independently of changes in cell-specific productivity between clarification runs, we plot the AAV-to-cell ratio of each sample collected, normalized by the cell-specific productivity, as supporting data in Fig. S6. This normalization renders the fold-increase in AAV per cell independent of upstream processing conditions, as cell-specific productivity is an upstream processing parameter with run-to-run variability. On average, the AAV-to-cell ratio rose by 5.4-fold (from pre- to post-microfluidic clarification) across the three experiments. Differences in the fold-increase of AAV-to-cell ratio across the three runs are affected by the sensitivity of the qPCR titer measurements and the cell density in the circulation loop, since that strongly dictates the degree of cell breakthrough to the harvest. We expect that variation in the titer readings is the most significant contributor to variation in the fold-increase of the AAV-to-cell ratio.

With three harvesting runs, we demonstrated that spiral microfluidic clarification achieves high AAV vector genome recoveries and effectively increases the AAV-to-cell ratio in the harvest stream by sequestering most cells to the circulation loop. Spiral microfluidic clarification can significantly reduce cell biomass and the burden those cells would have posed on subsequent processing steps. While genomic titers describe mass recovery from the primary harvest, evaluating full/empty capsid ratio and host-cell protein removal would be essential to define overall product quality.

3.4. Raising filter throughput by spiral microfluidic clarification to reduce downstream burden

We developed a harvest train that combines the unique strengths of spiral microfluidic clarification and conventional membrane filtration. Specifically, we processed material from the harvest stream of the spiral microfluidic device with a filter to determine if the efficiency of the overall harvest train benefited from the initial clarification performed with the inertial cell clarification system.

Identifying a filter's throughput is necessary for mapping a process volume to an appropriate filter membrane area. Depth filters typically clog with cells and cell debris, becoming unfit for further use once a specified volume of material, typically reported by the manufacturer, has passed through them. The pressure at the filter's inlet rises, and any further exertion on it could risk impurity breakthrough into

the harvest stream. Selecting an appropriate filter area for the corresponding process volume while simultaneously minimizing associated costs depends on the filter's throughput, which is measured as the volume of material processed across a cross-sectional area of the filter (L m^{-2}).

A filter throughput study shown in Fig. 6 was used to compare the HRC filter processing of crude cell culture material both with and without prior spiral device processing. These studies monitor the inlet pressure as material is passed through the HRC filter. Once the filtration cutoff inlet pressure is met, the throughput can be calculated from the total volume processed. The figure, which shows inlet pressure as a function of throughput with a filtration cutoff inlet pressure of 5 psi, indicates that the HRC filter achieved a throughput of 44.8 L m^{-2}, as 112 mL of material was processed through the 25 cm^2 HRC. Our result matches closely with an existing 40 to 50 L m^{-2} benchmark.[18] The HRC after spiral device processing achieved a higher throughput of 70 L m^{-2} at the same 5 psi cutoff, since 175 mL of material was processed through the 25 cm^2 HRC. This constitutes a 56.25% increase in the throughput of the HRC when spiral microfluidic clarification is first performed to remove most cells and cell debris before HRC use.

This presents a case for using spiral microfluidic technology and depth filtration in combination, as any opportunity to increase throughput could result in a significant increase in product recovery and decrease in costs. Furthermore, the two unit operations can be used in conjunction to provide a more thorough clarification, because the spiral device removes most of the cell mass that would otherwise excessively accumulate on the HRC filter's available surface area and block the Q-functionalized fibers from adsorbing unwanted host cell proteins and DNA. The spiral microfluidic device on its own would not be able to remove these smaller impurities, but our data do support that the removal of cell mass by spiral microfluidic clarification improves the depth filter's throughput. Thakur *et al.* report a 3-log reduction in host DNA content post-clarification with HEK293 cell culture lysates with a Harvest RC filter,[22] but for the current study, one limitation is that there is not enough information to conclude whether primary clarification with a spiral device leads to improved host cell protein and DNA removal with the secondary HRC filter.

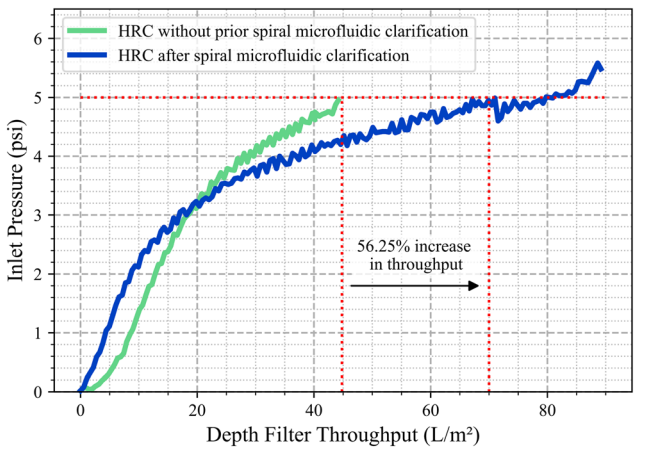

Fig. 6 Harvest RC (HRC) filter throughput study with and without prior spiral microfluidic device processing. Throughput (L m^{-2}) is measured as a function of inlet pressure (psi) to determine the throughput at the filtration cutoff of 5 psi. With prior spiral device processing, the throughput of the HRC filter rose by 56.25%.

The starting volume of the microfluidic-clarified solution for HRC processing was 320 mL, corresponding to two-thirds of the processable volume from Experiment 3. We selected this as a representative volume with a relatively low turbidity of less than 300 NTUs to compare with the initial cell culture, whose turbidity was too high for the meter to measure, at greater than 1000 NTUs. In the microfluidic-clarified solution, there was an estimated 2.04×10^{13} vg of recoverable vectors, which corresponded to a volume-weighted average AAV titer of 6.39×10^{10} vg mL^{-1}. The HRC filtrate had a titer of 5.42×10^{10} vg mL^{-1}, which means that the AAV recovery post-HRC is 84.9%. This is a good recovery for a 0.2 μm filter, which was presumably possible due to the primary clarification performed by the spiral microfluidic clarification step. A summary of these results is presented in Table S4.

3.5. Comparative analysis of AAV clarification strategies

Improving the recovery of an earlier step of downstream processing has a more pronounced effect on the overall process recovery than improving the recovery of a later step in downstream processing. For example, affinity chromatography columns have significantly lower vector recoveries when they are underloaded (*i.e.*, a poor AAV recovery post-clarification leads to fewer viral genomes entering the chromatography column, so it is underloaded).[24] Therefore, higher post-clarification vector recoveries permit bioprocessing teams to properly run affinity chromatography columns at the expected loading densities and achieve higher post-column recoveries.

Spiral microfluidic technology and the Harvest RC (0.2 μm) were used in series as two members of a harvest train, similarly to how Cecchini *et al.* used a 1.2 μm filter followed by a two-stage 0.8 μm/0.2 μm filter in their harvest train.[10] The spiral microfluidic device that we used and the 1.2 μm filter that they used were implemented to lower filter burden on a future downstream processing step, and the step recoveries for the initial clarification were 87.5% (from Experiment 3, Fig. 4(e)) and 44.7%,[10] respectively. When encountering the filter, the spiral device stack improved the AAV-to-cell ratio by 21.2× and removed a sufficiently high percentage of the cells that the HRC was able to recover AAVs with 84.9% recovery, when compared to the 73.7% recovery when Cecchini *et al.* used a 0.8 μm/0.2 μm filter for secondary clarification.[10] One nuance in this comparison is that in Cecchini *et al.*'s work, they used a lysed solution that was treated with nuclease prior to clarification, and those lysed components were trapped in the matrix of the 1.2 μm

filter, which worsened the unit operation's AAV recovery.[10] This comparative analysis was repeated with numerous one-stage and two-stage AAV clarification works, and summarized in Table 1.[10,11,25–27] Mendes *et al.* report the viral genome recoveries from batch culture as well as perfusion culture with alternating tangential flow (ATF) filtration and tangential flow depth filtration (TFDF).[11] Meierrieks *et al.* compare the recoveries from high-speed centrifugation (4000*g* for 30 minutes) and single-stage filtration with low-speed centrifugation (800*g* for 5 minutes).[25] McCarney *et al.* report recoveries from AAVs produced in adherent cell culture following two-stage clarification and vector concentration with a tangential flow filtration (TFF) membrane.[26] Turco *et al.* present a magnetic (membraneless) clarification strategy to collect AAVs from cell lysates.[27]

Processing rates for the studies in the comparison from Table 1 are listed when known. Assuming a filter operation with a 25 L m^{-2} prewash, a 40 to 50 L m^{-2} loading, a 5 to 10 L m^{-2} postflush, with a filter flux of 100 L m^{-2} per hour (LMH), filtration steps are approximately 42 to 51 minutes in duration.[18] Doria *et al.* harvested AAVs from a 1-unit CellSTACK culture (1 L volume), and compared the processing times between purifying the AAVs from cells (by lysis) and from medium (lysis-free).[28] They report a 63-hour duration for the lysis-based purification of AAVs from cells, which includes lysate preparation, two rounds of $CsCl_2$ purification, and desalting. They report a 3-hour duration for the purification of AAVs from medium, which includes 0.45 μm filtration and TFF.[28] To benchmark processing speed for 1 L of feedstock, we project that primary clarification using the 25-layer spiral microfluidic device would require 50 min. Secondary clarification of the liter with the HRC BC340 (340 cm^2 area) would require 18 min at a flux of 100 L m^{-2} per hour.

Spiral microfluidic devices rely on the hydrodynamic control of cells, rather than a physical barrier, to remove the majority of the feedstock's cell biomass. Among the technologies summarized in Table 1, this one is particularly suited for the primary clarification of non-lysed cell cultures where the target product has been secreted into the extracellular medium. Since lysates are polydisperse, with the debris spanning several orders of magnitude of size, the mixture of fragments, organelles, and other particles would likely fail to reach a common inertial focusing equilibrium position, and therefore a portion of that lysed material would be harvested through the outward outlet alongside the AAVs. Therefore, filters are currently a superior option for the clarification of intracellular AAVs from lysates.

We acknowledge that filters offer a near-guaranteed size cutoff which is contingent on maintaining transmembrane pressures within the manufacturer's limits, but the issues of clogging and fouling remain important challenges to address. The likelihood of a spiral channel becoming clogged is extremely low with typical cell suspensions, because the channel cross-sections are significantly larger than the pores of membrane-based filters. Cells do not deposit on the channel walls because they rarely come into contact with the walls at these fluid velocities. These advantages enable microfluidic clarification to be used for primary clarification within harvest trains involving large volumes, without the need to replace the device.

3.6. Manufacturing cost benefit analysis

Higher recoveries of AAVs lead to a larger number of doses produced per batch, which in turn lets bioprocessing teams recoup a larger fraction of their manufacturing costs, which include media and supplements, transfection or induction agents, and consumables. While it is difficult to calculate the exact cost–benefit of a higher product recovery, since different therapy formulations will be priced differently, product recovery is an important contributor to the cost per dose for both the patient and the manufacturer.

Another principal contributor to the manufacturing cost, the cost of filtration per unit volume, depends on the reciprocal of the throughput calculated in a filter throughput study and the price of the filter divided by the total membrane area.

$$\text{Clarification cost per liter}\left[\frac{\$}{\text{L}}\right] = (\text{Throughput})^{-1}\left[\frac{\text{m}^2}{\text{L}}\right]\cdot\text{Cost}_{\text{filter}}\left[\frac{\$}{\text{m}^2}\right]$$

Filter throughput depends on the input material. Since spiral microfluidic clarification was able to remove most of the cells and reduce the clarification burden downstream, the filter throughput increased. This, in turn, lowered product retention on the filter unit and lowered the cost of clarification per unit volume.

There is an inverse relationship between the filter cost per m^2 and the total membrane area. According to our analysis, low-capacity filters, designed to process 10 to 20 mL, are priced at over $100 per cm^2, whereas high-capacity filters, designed to process over 100 L, are priced at under $0.50 per cm^2. Our cost model, as shown in Fig. 7, serves as a map to determine the expected cost of filtration per liter of material, requiring only a starting volume and filter throughput as inputs. It accounts for the opportunity cost of using a filter that has too large a capacity for the task at hand.

The model incorporates filter cost per m^2 data and our filter throughput study results. It associates lower costs with higher throughputs and larger overall membrane areas. It includes other theoretical throughput values such as 20 L m^{-2}, 30 L m^{-2}, and 100 L m^{-2} for comparison. With multiple filter throughput studies, it is possible to add multiple filter types and sizes with their projected throughputs onto the graph to identify the optimal option.

The data points used to generate these plots were fit to power law relationships of the form $y = a{\cdot}x^b$ at throughputs ranging from 10 to 100 L m^{-2} in Fig. S7. This methodology can be used to map a throughput value and process volume

Table 1 Comparison of one-stage and two-stage clarification strategies for AAV downstream processing. Overall recoveries are calculated by multiplying the recovery from primary clarification with the recovery from secondary clarification or simply using the recovery from primary clarification when there is no secondary clarification. Abbreviations: Sf9, *Spodoptera frugiperda*; rAAV, recombinant AAV; qPCR, quantitative PCR; ddPCR, droplet digital PCR; ELISA, enzyme-linked immunosorbent assay; ATF, alternating tangential flow; TFDF, tangential flow depth filtration; TFF, tangential flow filtration; HF, hollow fiber TFF; FSO, flat sheet omega TFF; FSD, flat sheet delta TFF. Products: 3M Harvest RC (0.2 μm) (3M, USA); Sartopure GF Plus Maxicaps (1.2 μm) (Sartorius Stedim Biotech, Germany); Sartopore 2 XLG (0.8 μm/0.2 μm) (Sartorius Stedim Biotech, Germany); ULTA GF (5.0 μm) (Cytiva, USA); XCell ATF (0.5 μm) (Repligen Corporation, USA); KrosFlo TFDF (5.0 μm) (Repligen Corporation, USA); Millistak+ HC Pro Pod X0SP (0.1 μm) (MilliporeSigma, USA); Sartolab RF 50 (0.22 μm) (Sartorius AG, Germany); Stax capsule with PDK11 media (1.0 to 20 μm) (Pall Corporation, USA); Supor EKV membrane in Kleenpak capsules (0.2 μm) (Pall Corporation, USA); MidGee hoop ultrafiltration hollow fiber cartridges (Cytiva, USA); Cadence single-use flat sheet omega (Cytiva, USA); T-series flat sheet delta (Cytiva, USA)

	This study	Cecchini *et al.*, 2011 (ref. 10)	Mendes *et al.*, 2022 (ref. 11)			Meierrieks *et al.*, 2023 (ref. 25)		McCarney *et al.*, 2025 (ref. 26)	Turco *et al.*, 2023 (ref. 27)
Available information on cell culture and vectors	Suspension human producer cells, proprietary AAV	Suspension Sf9 cells, unspecified rAAV	Suspension HEK293T cells, AAV8			Suspension HEK293 cells, AAV2 and AAV5		Adherent HEK293A, AAV5	Suspension HEK293T, rAAV5
Lysis Titer assessment	No lysis Genomic titer (qPCR)	Lysis Genomic titer (qPCR), capsid recovery (western blot)	Lysis Genomic titer (qPCR), capsid titer (ELISA)			Lysis Genomic titer (ddPCR), capsid titer (ELISA)		Lysis Genomic titer (ddPCR), capsid titer (ELISA)	Lysis Genomic titer (qPCR), capsid titer (Gyrolab AAVX kit)
Primary clarification method	Spiral microfluidics	Sartopure GF plus Maxicaps (1.2 μm)	ULTA GF (5.0 μm)	XCell ATF (0.5 μm)	KrosFlo TFDF (5.0 μm)	Centrifugation (4000*g*, 30 minutes)	Sartolab RF 50 (0.22 μm)	Stax capsule with PDK11 media (1.0 to 20 μm)	Magnetic separator
Primary clarification recovery (%)	87.5 (Experiment 3), 85.1 (mean)	44.7	91	39 (mean), 61 (max)	61.7 (mean), 97 (max)	32 (AAV2), 84.9 (AAV5)	42.6 (AAV2), 86.9 (AAV5)	—	63
Primary clarification speed (mL min^{-1})	20, 0.2 per spiral	—	—	22.5	22.5	1.7	40 to 55 (clogs)	—	47
Primary clarification loading (L m^{-2})	—	83.3	23	16 to 25	—	—	4.8	—	—
Secondary clarification method	Harvest RC BC25	Sartopore 2 XLG (0.8 μm/0.2 μm)	Sartopore 2 XLG (0.8 μm/0.2 μm)	—	Sartopore 2 XLG (0.8 μm/0.2 μm) or Millistak+ HC Pro Pod X0SP (0.1 μm)	—	—	Supor EKV membrane in Kleenpak capsules (0.2 μm)	—
Secondary clarification recovery (%)	84.9 (Experiment 3)	73.7	82	—	78 (Sartopure), 92 (Millistak)	—	—	—	—
Secondary clarification loading (L m^{-2})	70	125	30	—	33 (Sartopure), 64 (Millistak)	—	—	—	—
Overall clarification recovery (%)	74.3	32.9	74.6	39	48.1 (Sartopure), 56.8 (Millistak)	32 (AAV2), 84.9 (AAV5)	42.6 (AAV2), 86.9 (AAV5)	82.3 (HF), 82.2 (FSO), 75.4 (FSD)	63
Notes	AAVs left behind in the bulk fluid of the circulation loop during primary clarification are reported as losses	Loadings are calculated from reported filter volumes used per liter of lysate	Mean and maximum values from primary clarification are reported			Recoveries are calculated relative to the genomic titer of the control condition (harvest material after centrifugation at 800*g* for 5 minutes). Each batch processed is 50 mL, unless clogging occurred		Recoveries are reported after a TFF concentration step with HF, FSO, or FSD TFF membranes	Clarification speed is calculated as the quotient of processing volume and processing time

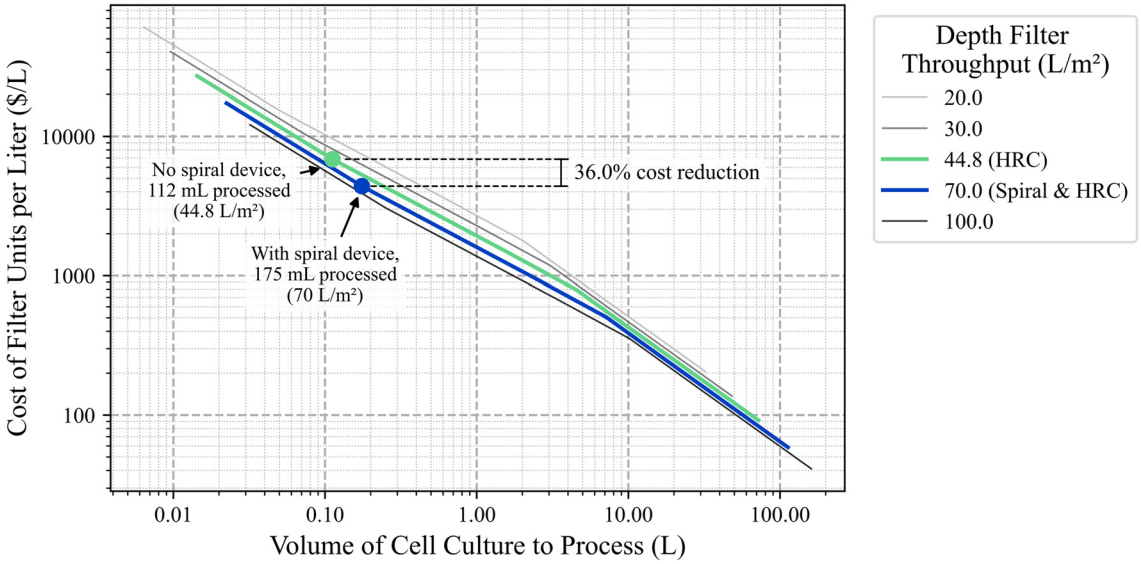

Fig. 7 A cost model of the relationship between the per-liter cost of Harvest RC (HRC) filters and the volume of cell culture processed at different throughputs between 20 and 100 L m^{-2}. The two points on the graph show the results of the filter throughput study (on the 44.8 L m^{-2} and 70 L m^{-2} lines) and the corresponding expected per-liter cost reduction of 36.0%. All other throughputs graphed are theoretical. Pricing data comes from the following HRC units: BC4, BC25 Sanitary, BC340, BC1020, BC2300, and BC16000.

to an expected cost per liter. The curve for HRC processing without prior spiral microfluidic clarification, with a throughput of 44.8 L m^{-2}, has a fitted power law equation of $y = 1667 \cdot x^{-0.657}$ and the curve for HRC processing after microfluidic clarification with a throughput of 70 L m^{-2} has a fitted power law equation of $y = 1430 \cdot x^{-0.657}$. Improving the throughput of the unit operation enables a user to move from one power law curve to a different, more advantageous one.

Another important consideration for this study was identifying a normalization unit for both filtration-based and membraneless technologies. In the HRC filter throughput study presented in Fig. 6, filter efficiency is measured using its throughput. This metric is used to normalize the filter's performance by its area (*i.e.*, having its performance reported per m^2 of filter area). All other variables were held equal; a larger filter membrane area can process a larger volume of cell culture material before getting clogged.

In contrast, spiral microfluidic technology does not have a membrane area that the operation can be normalized with respect to, so instead, the unit used to normalize microfluidic clarification is the number of spirals used in the multiplexed device stack. The inertial focusing events occurring in each of the 100 parallelized spirals are independent of each other, so it would be appropriate to normalize the operation by the number of spirals used to perform it. If all other variables are held equal, a larger number of spirals allows a harvesting routine to be performed more rapidly. The number of spirals primarily affects the duration of the harvesting run. One spiral can accomplish the entire harvest on its own, but it would take significantly more time to complete than it did in our harvesting runs. This dichotomy between how filter-based downstream processing is normalized by filter area and how spiral microfluidic-based downstream processing is normalized by spiral number highlights the cost advantages and operational flexibility of using spiral microfluidic technology for industry-scale processes. Plastic microfluidic chips are a fixed cost in relation to cell culture volume, and cost less than $1 per device. Filtration technologies are a variable cost in relation to cell culture volume because of their reliance on filter area (Fig. 7). If lowering processing time and raising throughput is crucial, then the number of spirals used to build the multiplexed spiral microfluidic device stack can be raised to reduce overall cell clarification time.

3.7. Computational fluid dynamics modeling of the flow profile

Spiral microfluidic device-mediated removal of cells relies on a balance of Dean drag and inertial lift forces to create a focusing band near the inner wall of the spiral channels. We performed computational fluid dynamics (CFD) simulations to provide a theoretical model for operating the device. In a one-layer device fluid flow and particle tracing simulation, particles enter through the inlet and the focusing band tightens as the cells travel through the four loops (Fig. S8(a)). The velocity profile at the centerline and the pressure profile along the exterior walls are shown in Fig. S8(b) and (c), showing a maximum fluid velocity of 1 m s^{-1} and a pressure differential from the inlet to outlet of ~34 kPa. A cross-section of the channel showing the secondary fluid velocity components reveals the characteristic counter-rotating Dean vortices formed during Dean flow (Fig. S8(d) and (e)). Channel deformation is expected to be negligible since the device is built from plastic. Calculations supporting this are available in the SI.

From the CFD simulation of the 25-layer device, the pressure at the top layer's inlet was 35.0 kPa and the pressure at the bottom layer's inlet was 35.6 kPa (Fig. S9(c)). This corresponds to a 1.7% difference between the pressures at these layers' entrances. This difference in pressure is relatively small compared to the ~35 kPa pressure differential between any layer's inlet and outlets; however, the computed flow rates within each layer deviate slightly from their theoretical value. The inlet flow rate of 1000 mL min^{-1} divided between 100 spirals had simulated flow rates varying between 9.89 and 10.12 mL min^{-1} per spiral, compared to a theoretical flow rate of 10 mL min^{-1} per spiral (≤1.23% error, Fig. S9(d)). We expect inertial focusing performance to remain unaffected within this range of flow rates.

The residence time for one pass through the device is less than 0.4 seconds. The flow-weighted average shear rate in the 25-layer spiral device is 5604.8 s^{-1} (with calculation details in the SI). This computed shear rate compares closely with other clarification technologies such as a TFDF which operates at shear rates between 4000 and 6000 s^{-1}.[11] AAVs are also expected to be stable under these conditions with the ability to withstand shear rates up to 20 000 s^{-1}.[29]

4. Conclusions

We utilized a spiral inertial microfluidic platform to perform primary clarification of cell culture feedstocks, while focusing on AAV genomic recoveries and cell removal rates to evaluate device performance. The 25-layer spiral device harvested AAVs at a respectable 20 mL min^{-1} and achieved an average AAV genomic recovery of 85.1% or higher, with an average cell removal rate of 80.4%. The removal of most of the cell biomass from the initial feedstock by spiral microfluidic clarification reduced downstream burden on the secondary 0.2 μm 3M HRC filter. This resulted in a more efficient utilization of the secondary filter's surface area, which enhanced the filter throughput by 56.25%, reduced filtration costs by 36%, and led to a step recovery of 84.9%.

Future strategies to explore include optimizing the microfluidic device designs or process optimization by adding media or additional cell culture to the retention flask to reduce the cell density in the harvest stream and prolong low-loss AAV harvests. Portions of the harvest with higher-than-desirable cell densities and cell breakthrough can be processed multiple times using the same device.

Author contributions

Alexander Bevacqua: conceptualization, formal analysis, investigation, methodology, validation, visualization, writing – original draft, writing – review & editing. Do Hyun Park: conceptualization, investigation, methodology, validation. Sheryar Khan: investigation, methodology. Qingxuan Li: investigation, methodology. Mahsa Hadidi: conceptualization, funding acquisition, project administration, resources, supervision, writing – review & editing. Jianzhu Chen: conceptualization, funding acquisition, project administration, resources, supervision, writing – review & editing. Jongyoon Han: conceptualization, funding acquisition, project administration, resources, supervision, writing – review & editing.

Conflicts of interest

There are no conflicts of interest to declare.

Data availability

The data supporting this article have been included as part of the supplementary information (SI).

Supplementary information is available. See DOI: https://doi.org/10.1039/d5lc01050k.

Acknowledgements

The authors thank Hyungkook Jeon (Seoul National University of Science and Technology, and formerly, MIT) for the original microfluidic device design as well as Junghyo Yoon (MIT) and Taehong Kwon (MIT) for assisting Hyungkook with the original design of the cell clarification platform. This work is the result of a collaborative agreement between MIT and Sanofi, and it is additionally supported by the National Science Foundation Graduate Research Fellowship Program under Grant 2141064 and the US Food and Drug Administration under Grant 1R01FD007480-03. Any opinions, findings, and conclusions or recommendations expressed in this material are those of the authors and do not necessarily reflect the views of the National Science Foundation, the US Food and Drug Administration, or Sanofi.

References

1 H. K. E. Au, M. Isalan and M. Mielcarek, *Front. Med.*, 2022, **8**, 1–14, DOI: 10.3389/FMED.2021.809118.
2 W. Shen, S. Liu and L. Ou, *Front. Immunol.*, 2022, **13**, 1–13, DOI: 10.3389/FIMMU.2022.1001263.
3 Z. Zhao, A. C. Anselmo and S. Mitragotri, *Bioeng. Transl. Med.*, 2022, **7**, 1–20, DOI: 10.1002/BTM2.10258.
4 T. Travieso, J. Li, S. Mahesh, J. D. F. R. E. Mello and M. Blasi, *npj Vaccines*, 2022, **7**, 1–10, DOI: 10.1038/S41541-022-00503-Y.
5 L. H. Vandenberghe, R. Xiao, M. Lock, J. Lin, M. Korn and J. M. Wilson, *Hum. Gene Ther.*, 2010, **21**, 1251–1257, DOI: 10.1089/HUM.2010.107.
6 Z. Jiang and P. A. Dalby, *Trends Biotechnol.*, 2023, **41**, 1268–1281, DOI: 10.1016/J.TIBTECH.2023.04.002.
7 E. M. Atkinson, V. P. Fung, P. C. Wilkins, R. K. Takeya, T. C. Reynolds and I. L. Aranha, Methods for generating high-titer, helper-free preparations of recombinant AAV vectors, *US Pat.*, US6995006B2, 2006.

8 A. Srivastava, K. M. G. Mallela, N. Deorkar and G. Brophy, *J. Pharm. Sci.*, 2021, **110**, 2609–2624, DOI: 10.1016/J.XPHS.2021.03.024.
9 S. B. Wang, S. Godfrey, F. Radoniqi, H. Lin and J. Coffman, *Biotechnol. J.*, 2019, **14**, 1–6, DOI: 10.1002/BIOT.201800137.
10 S. Cecchini, T. Virag and R. M. Kotin, *Hum. Gene Ther.*, 2011, **22**, 1021–1030, DOI: 10.1089/HUM.2010.250.
11 J. P. Mendes, B. Fernandes, E. Pineda, S. Kudugunti, M. Bransby, R. Gantier, C. Peixoto, P. M. Alves, A. Roldão and R. J. S. Silva, *Front. Bioeng. Biotechnol.*, 2022, **10**, 1020174, DOI: 10.3389/FBIOE.2022.1020174.
12 H. Jeon, T. Kwon, J. Yoon and J. Han, *Lab Chip*, 2022, **22**, 272–285, DOI: 10.1039/D1LC00995H.
13 M. E. Warkiani, A. K. P. Tay, G. Guan and J. Han, *Sci. Rep.*, 2015, **5**, 1–10, DOI: 10.1038/SREP11018.
14 T. Kwon, H. Prentice, J. De Oliveira, N. Madziva, M. E. Warkiani, J.-F. P. Hamel and J. Han, *Sci. Rep.*, 2017, **7**, 6703, DOI: 10.1038/S41598-017-06949-8.
15 A. Bevacqua, F. Liu, J. Chen and J. Han, *Lab Chip*, 2026, **26**, 2368–2379, DOI: 10.1039/D6LC00029K.
16 M. Leach, K. Edmonds, E. Ingram, R. Dutch, R. Wickramasinghe, M. Chwatko and D. Bhattacharyya, *NANO*, 2025, **15**, 310, DOI: 10.3390/NANO15040310.
17 3M, 3M™ Harvest RC Specification Sheet, https://multimedia.3m.com/mws/media/1990588O/3m-harvest-rc-brochure.pdf, (accessed 4 March 2024).
18 M. T. Park, A. Verma, C. A. Froelich and S. P. Motevalian, *Trends Biotechnol.*, 2025, **43**, 1921–1937, DOI: 10.1016/J.TIBTECH.2025.02.016.
19 K. Choi, H. Ryu, K. J. Siddle, A. Piantadosi, L. Freimark, D. J. Park, P. Sabeti and J. Han, *Anal. Chem.*, 2018, **90**, 4657–4662, DOI: 10.1021/ACS.ANALCHEM.7B05200.
20 D. C. Yeo, C. Wiraja, Y. Zhou, H. M. Tay, C. Xu and H. W. Hou, *ACS Appl. Mater. Interfaces*, 2015, **7**, 20855–20864, DOI: 10.1021/ACSAMI.5B06167.
21 R. Chinnawar and N. Marchand, *Cell Gene Ther. Insights*, 2022, **8**, 483–493, DOI: 10.18609/CGTI.2022.070.
22 G. Thakur, S. Mink, H. Bak and A. D. Tustian, *Sep. Purif. Technol.*, 2025, **354**, 128557, DOI: 10.1016/J.SEPPUR.2024.128557.
23 M. Mayani, S. Nellimarla, R. Mangalathillam, H. Rao, S. Patarroyo-White, J. Ma and B. Figueroa, *Biotechnol. Prog.*, 2023, 1–12, DOI: 10.1002/BTPR.3409.
24 J. Heckel, T. Bohlig, L. Bonnington, M. Leiss, M. Haindl, J. Hubbuch and T. Graf, *Biotechnol. J.*, 2025, **20**, e202400656, DOI: 10.1002/BIOT.202400656.
25 F. Meierrieks, A. Pickl and M. W. Wolff, *J. Biotechnol.*, 2023, **367**, 31–41, DOI: 10.1016/J.JBIOTEC.2023.03.010.
26 L. McCarney, A. Gutha Ravichandran, S. Tansey, M. Dango and N. Marchand, *Sep. Purif. Technol.*, 2025, **370**, 133064, DOI: 10.1016/J.SEPPUR.2025.133064.
27 F. Turco, A. Wegelius, O. Lind, N. Norrman, A. C. Magnusson, C. Sund-Lundström, B. Norén, J. Hedberg and R. Palmgren, *Mol. Ther. - Methods Clin. Dev.*, 2023, **30**, 394–402, DOI: 10.1016/J.OMTM.2023.07.010.
28 M. Doria, A. Ferrara and A. Auricchio, *Hum. Gene Ther. Methods*, 2013, **24**, 392–398, DOI: 10.1089/HGTB.2013.155.
29 A. Picciano, K. Wilson, K. Joyner and M. Wendeler, *J. Pharm. Sci.*, 2025, **114**, 104017, DOI: 10.1016/J.XPHS.2025.104017.